Electrospun Fibrinogen/PLA Nanofibers for Vascular Tissue Engineering

D. Gugutkov, [1] J. Gustavsson, [1] M. Cantini,[2] M.Salmeron-Sánchez [2] and G. Altankov [1, 3, 4] *

[1] *Institute for Bioengineering of Catalonia (IBEC), Barcelona, Spain*

[2] *Division of Biomedical Engineering, School of Engineering, University of Glasgow, Glasgow G12 8LT, United Kingdom*

[3] *Centro de Investigación Biomédica en Red en Bioingeniería, Biomateriales y Nanomedicina (CIBER-BBN), Zaragoza, Spain*

[4] *ICREA (Institucio Catalana de Recerca i Estudis Avançats), Spain*

* *Author to whom correspondence should be addressed:*

george.altankov@icrea.cat; Tel: +34 93 403 97 09; Fax: +34 93 403 98 73

.

Abstract

Here we report on the development of new type hybrid fibrinogen/polylactic acid (FBG/PLA) NFs with improved stiffness combining the good mechanical properties of PLA with the excellent cell recognition property of native FBG. We were particularly interested on the dorsal and ventral cell response to the nanofibers organization - random or aligned - using human umbilical endothelial cells (HUVEC) as model system. Upon ventral contact with random NFs the cells developed a stellate-like morphology with multiple projections. The well-

developed focal adhesion complexes suggest a successful cellular interaction. Time-lapse analysis however shows significantly lowered cell movements resulting in relatively short distance that they traverse in multiple directions. Conversely, an elongated cell shape and significantly increased cell mobility were observed on aligned NFs. To follow the dorsal cell response artificial wounds were created on confluent cell layers previously grown on glass slides and covered with either random or aligned NFs. Time-lapse analysis showed significantly faster wound coverage (within 12 h) of HUVECs on aligned samples vs. almost absent directional migration on random ones. However, nitric oxide (NO) release shows that endothelial cells possess lowered functionality on aligned NFs compared to random ones, where significantly higher NO production was found. Collectively, our studies show that randomly organized NFs could support the endothelization of implants while aligned would rather direct cell locomotion for guided neovascularization.

1. Introduction

The reconstruction of an altered tissue or organ by bioengineered scaffolds seeded with living cells holds enormous promise (Dvir et al, 2010) which particularly relates to the purposes of today's vascular tissue engineering (Cleary et al, 2012). The use of synthetic conduits for development of artificial vessels however is severely limited by their insufficient coverage with endothelial cells, often resulting in graft failure, which particularly relates to small diameter arteries (Cleary et al, 2012). It urgently calls for development of novel constructs resembling the natural architecture of the vessel wall where cells can grow and remodel their extracellular matrix (ECM) (Cleary et al, 2012). It is widely appreciated that the geometry of the surrounding matrix is a key parameter to engineer tissues. Indeed, distinct organizational features (Arnold et al 2004) including adhesive micro- and nano-patterns (Dvir et al 2010; Thery et al 2006) are strongly influential in directing cell behavior and functionality (Wade and Burdick, 2012). Most of these studies however involve planar substrates which are ideal for characterizing morphological cell response but lack the real three-dimensional (3D) architecture necessary for the establishing of a functional tissue (Dvir et al 2010). Conversely, studies on cells encapsulated in hydrogel systems provide adequate 3D microenvironment but lack the hierarchical fibrillar organization of ECM and its mechanical properties (Lutolf and Hubbell, 2005; Dvir et al 2010). Fibrillar structures provoke the cellular interaction apart from providing better mechanical support. They can also guide a directional cell movement (Dvir et al 2010). Therefore the

implication of electrospining technology for producing fibrous scaffolds have received much attention in tissue engineering due to the morphological and dimensional similarity of produced nanofibers to the natural ECM (recently reviewed by Liu et al, 2013). Moreover, during electrospinning the nanofibers can be oriented depending on the fiber collection setup (Baji et al 2010) and recent studies have shown that such oriented nanofibers can guide the spatial arrangement of cytoskeletal proteins resulting in their elongation along the fibers orientation (Liu et al 2009; Guelcher and Goldstein, 2009). However, relatively little is known whether fibers orientation can influence the overall cell behavior and cell-specific functionality (Fu and Wang, 2012), particularly of endothelial cells, which are a principal cellular component of the vessel wall (Fang et al, 2011).

Current studies in the field show that nanofibrous scaffolds should be considered as ideal candidate for the engineering of the vessel wall because they mimic the fibrillar structure of ECM (Ma et al 2002; Steven and George, 2005; Swartz et al 2005), provide the desired mechanical stability (Edelman, 1999) and topographical features that encourage endothelial cells interaction and growth (Chiu et al, 2005; Nisbet et al 2007; Kuar and Krishnan, 2001).

Utilizing established protocols (Wenek et al 2003; He et al 2011; Perumcherry et al, 2011) previously we have electrospun native fibrinogen (FBG) nanofibers (NFs) considering distinct *in vitro* studies on cell behavior and potential vascular tissue engineering application (Gugutkov et al, 2013). Though these fibers were well-recognized by endothelial cells, they presented poor mechanical properties being too soft and easy breakable in contact with cells. Here we report on the

development of novel type hybrid fibrinogen/polylactic acid (FBG/PLA) nanofibers with improved mechanical properties, but retaining at the same time the good cell-recognition characteristics of the native FBG. This paper describes some aspects of their production and biological characterization emphasizing the role of NFs organization upon contact with the dorsal or ventral cell surfaces, using human umbilical endothelial cells (HUVEC) as a relevant cell model.

2. Materials and Methods

2.1 Electrospinning of FBG/PLA nanofibers

For production of composite FBG/PLA nanofibers, fibrinogen from bovine plasma (Sigma-Aldrich) and poly-L-DL-lactic acid 70:30 (PURAC) were separately dissolved in 1-1-1-3-3-3-hexafluoroisopropanol (HFIP; Sigma-Aldrich). PLA (4% w/v) was dissolved overnight at room temperature under continuous agitation. Fibrinogen (100 mg ml^{-1}) was dissolved in a 9:1 mixture of HFIP and 10x DMEM (Invitrogen) and centrifuged at 4000 rpm for 10 minutes. The supernatant was carefully collected, mixed with the PLA solution (1:1 v/v) and loaded in a syringe pump (AITECS). For electrospinning we used a conventional setup based on a high voltage supply (Glassman High Voltage Inc.) and a grounded collector. Randomly deposited nanofibers were obtained by vertical electrospinning onto 15 mm round shaped glass coverslips (Thermo Scientific) placed on aluminum foil. Aligned fibers were obtained using an original method of collection as recently described (Gugutkov et al 2013). The applied voltage in both cases was 25–30 kV, the distance between the needle tip and the collector was 125 mm, and the pump flow rate was set to 0.5 ml h^{-1}.

2.2 Characterization of nanofibers

2.2.1 Fiber morphology and alignment

The electrospun FBG/PLA fibers were coated with a conductive layer of sputtered gold, and then viewed by scanning electron microscopy (SEM) at 15 kV (JeolJSM-5410). Fast Fourier transformation (FFT) outputs of the SEM micrographs were used to characterize fiber alignment (ImageJ with Oval profile

plug-in). Briefly, a circular projection was placed on the FFT frequency distribution outputs and the radial sums of the pixel intensities for each angle (0 to 180°) was calculated. Pixel intensity was then plotted as a function of its angle of acquisition. Distribution data was normalized to a baseline value and plotted in arbitrary units.

2.2.2 Atomic Force Microscopy

Nanofibers of different composition (composite FBG/PLA, pure FBG, and pure PLA, respectively) were incubated at 37 °C in PBS for either one day or one week to characterize their stability. After incubation, the fibers were dried under nitrogen flow and their morphology and mechanical properties were evaluated using atomic force microscopy (AFM). For that purpose, the Nanowizard® 3 Bioscience AFM (JPK Instruments AG) was used in the quantitative imaging (QI™) mode with a setpoint of 0.4 V, a *Z* length of 0.7 µm, and an extend/retract time of 7 ms. Cantilevers with a spring constant of 2.8 N/m (Bruker) were used. The height, slope and adhesion images were obtained from the force spectroscopy curves recorded for each pixel of the scanned areas (256 x 256 pixels).

The mechanical properties of the nanofibers, namely their stiffness, were measured through nanoindentation experiments performed via AFM. Nanoindentations were carried out in a MultiMode AFM from Bruker (Billerica, MA) using cantilevers (OTR8 from Bruker) with a 0.57 N/m spring constant and a square pyramidal tip with half-angle of 35º. Calibration of the tip sensitivity was performed in the same conditions as the experiments using a flat rigid surface and the value was used to correct the force-height curves for the

deflection of the cantilever. The stiffness was then calculated using the slope of the force-penetration curves as described elsewhere (Forner et al. 2009).

2.2.3 Stability

To determine the stability of FBG-containing nanofibers in aqueous surrounding we labeled FBG with fluorescein isothiocyanate (FITC) (0.1 mg ml^{-1}) before electrospinning. Nanofibers containing known amounts of FITC-FBG (0.2% from the total protein) were then electrospun in controlled quantities (1.0 mg), and thereafter incubated at 37 °C in PBS for up to 72 hours. After incubation, the supernatant was collected and its fluorescence was measured (494 nm excitation, 525 nm emission; FluoroMax-4, Horiba-Jobin Yvon). Pure FBG nanofiber samples obtained as previously described (Gugutkov et al 2013), containing the same amount of FITC-labeled FBG, were used as control.

2.3 Cells

Human umbilical vein endothelial cells (HUVECs) were obtained from MilliPore and cultured in complete EndoGRO medium (MilliPore) with 2% fetal bovine serum (FBS). For experiments, cells were harvested with trypsin/EDTA which subsequently was inactivated by FBS and washed twice in FBS-free medium. Cells were seeded on nanofiber samples placed in standard 24 well plates, using typically 2.0 ml medium.

2.3.1 Cell morphology and visualization of focal adhesion complexes

Overall cell morphology on randomly and aligned electrospun FBG/PLA nanofibers was evaluated after two hours of incubation in serum-free conditions (cell seeding density: 5 x 10^4 cells per sample), and also after seven days of incubation in presence of FBS (cell seeding density: 3 x 10^4 cells per sample). After incubation, cells were washed with PBS, fixed with 4% paraformaldehyde, permeabilized with 0.5% Triton-X100, and stained with FITC-phalloidin (Invitrogen) for actin cytoskeleton and Hoechst 34580 (Invitrogen) for nuclei. Focal adhesions were visualized with monoclonal anti-vinculin antibody (Sigma-Aldrich) followed by goat anti-mouse AlexaFluor® 555-conjugated secondary antibody (Abcam). Cells were photographed using an inverted fluorescent microscope (Axio Observer Z1, ZEISS) and at least three representative images were acquired for each sample condition.

2.3.2 Nitric oxide production

A nitric oxide assay kit (Enzo, Life Science) based on the Griess reaction was used to colorimetrically determine total nitrate levels in the culture supernatants after one and three days of cell culturing on random and aligned FBG/PLA nanofibers. As no significant difference in cell growth was found between random, aligned and a control sample (glass coated with 50 µg/ml FBG at 37ºC for 30 min) after 7 days of culture, direct comparison of the photometric signals without normalization to cell numbers was done.

2.3.3 Long-term cultures

To follow long-term cell response to random and aligned nanofibers, 3 x 10^4 cells were seeded on the samples and cultured for seven days in complete

EndoGRO medium that was exchanged each second day. At the end of incubation the cells were fixed and stained for actin and nuclei as described above. In addition, cell-produced fibronectin (FN) matrix was visualized by immunofluorescence using polyclonal anti FN antibody (Sigma, Cat. No. F3648) followed by AlexaFluor® 555 anti-rabbit secondary antibody (Invitrogen, Cat. No. A21428). Cell density was determined by counting the cell nuclei in four randomly chosen squares from low magnification fluorescent images.

2.3.4 Cell mobility

To investigate how FBG/PLA nanofibers influence cell mobility we distinguished between dorsally and ventrally applied nanofibers. In the latter case, time-lapse recordings of HUVECs were initiated one hour after cell seeding (3 x 10^4 cells per sample) on FBG/PLA nanofibers and proceeded for six hours (12 images per hour) using an on-stage mini-chamber coupled to the microscope (Axio Observer Z1, Zeiss) to assure appropriate cell culture conditions (37°C, humidified atmosphere and 5% CO_2). To investigate the dorsal cell response to nanofibers, confluent layers of HUVECs produced on glass slides were scratched with a sterile pipette tip to produce an artificial wound (ca 1 mm wide). Cells layer were then covered with random or aligned nanofibers deposited onto 10 mm cylindrical Teflon rings to ensure intimate contact of cells with nanofibers and recorded as above for up to 12 hours. Time-lapse recordings were processed using the MTrackJ plugin of ImageJ (developed by Biomedical Imaging Group of the Erasmus University Medical Center Rotterdam, Netherlands). Path trajectories of 15 (ventral experiment)

and 20 (dorsal experiment) randomly chosen cells were traced manually following their position at each 10^{th} frame of the time-laps records to analyze their motile behavior.

2.4 Statistical analysis

Data are expressed as mean ± standard deviation (SD) if not indicated otherwise. Statistical significance was determined by two-tailed independent Student's t-test ($p < 0.05$).

3. Results

3.1 Morphology and mechanical properties of electrospun FBG/PLA nanofibers

Composite FBG/PLA nanofibers were obtained by electrospinning a mixture of FBG and PLA in HFIP collected as a homogenous layer of either random or aligned fibers (Fig. 1 A, B). In the latter case, pixel intensity distribution obtained from FFT analyses of representative SEM fiber images revealed that majority of the fibers aligned within 10° of the major fiber direction (Fig.1 C, D). The main fibers diameter determined from SEM images is shown at Fig. 1 E. It was: 398 ± 128 nm for random fibers and 250 ± 160 nm for aligned ones (n = 100). The mechanical properties of dry nanofibers were determined by nanoindentations using AFM. Fig. 1 F shows that reinforcement of FBG nanofibers with PLA substantially increased the local stiffness of the fibers from 30 ± 10 Nm^{-1} to 275 ± 50 Nm^{-1}. Meanwhile, pure PLA fibers were significantly stiffer than composite nanofibers (4000 ± 400 Nm^{-1}).

3.2 Stability of electrospun fibers in physiological solution

The stability of composite and pure nanofibers in aqueous solutions was initially estimated from morphological changes using AFM. After seven days of incubation (PBS at 37 ºC), both FBG and PLA/FBG fibers presented clear changes in their morphology as judged from AFM adhesion strength magnitude images. Over the same period, pure PLA fibers remained unaltered (Fig. 2). AFM height images however did not reveal any significant differences on surface roughness suggesting less sensitivity of this approach, but also implying that degradation is rather negligible. No evidence for degradation was found at intermediate times (data not shown) indicating that samples were unaltered at shorter periods of incubation. Fiber stability was further characterized by measuring fluorescent release from electrospun FBG/PLA composite fibers containing FITC-FBG. For comparison, pure FBG nanofibers containing the same amount of FITC-FBG (0.2% from the total protein) and prepared according previously described protocol were used (Gugutkov et al. 2013). As shown on Fig. 3 the fluorescent signal in the supernatant gradually increased with the incubation time, and the kinetics of FITC-FBG release was very similar for pure FBG and composite FBG/PLA nanofibers.

3.3 Cellular response upon ventral contact with FBG/PLA nanofibers

The response of HUVECs to ventral contact with composite nanofibers was first evaluated morphologically in a short-term experiment. After two hours of incubation, adhesion to random nanofibers promoted an irregular cell shape with multiple cytoplasmic projections extending towards differently oriented

fibers (Fig. 4 A and C). The cell protrusions showed high accumulation of actin that co-localized with vinculin in focal adhesions (Fig. 4 C) where long actin fibers with centripetal organization inserted, suggesting firm adhesive interaction with fibers. On aligned fibers (Fig. 4 B, D), cells acquired an extended morphology that strongly follows the fibers orientation. The highly extended actin stress fibers inserted into well-developed focal adhesion complexes (Fig. 4 D) indicate that cells exercised traction over the nanofibers. Time-lapse recordings further demonstrated that HUVECs were highly motile on aligned FBG/PLA nanofibers (Suppl. video 1) with individual cells undergoing the typical motile cycle of extending a leading cell edge, followed by traction of the tail cell edge. While most of the cells on aligned FBG/PLA nanofibers carried out a linear path of translocation (Fig. 4 F), tracking analysis of cell motion (Suppl. video 2) showed that cells on random nanofibers performed restricted movements in arbitrary directions (Fig. 4 E) resulting in shorter travelled distance compared to cells on aligned nanofibers.

3.4 Cellular response to dorsal contact with FBG/PLA nanofibers

To study the cellular response to dorsal application of PLA/FBG nanofibers (i.e., 3D response), we overlaid random or aligned nanofibers on artificial wounds created in confluent cell layers and then recorded cell migration (Suppl. video 3 and 4). Tracking analysis revealed that HUVECs moved without any preferred direction, i.e. showing disoriented migration within 12 hours of recording, when coated with random nanofibers (Fig. 5 A and C). As a consequence, the cells traversed relatively short distances on random fibers, and remained near the altered wound edges. Conversely, when cells were

covered with aligned nanofibers (Fig. 5 B and D) they were confined to traverse significantly longer distances resulting in uniform wound coverage within 12 hours.

3.5 Long-term cell culture on FBG/PLA nanofibers

No significant difference in cell growth was found between random and aligned, as well as control samples of FBG-coated glass substrata even after 7 days of culture (see Table 1). Fiber orientation was however observed to affect both cellular organization and ECM deposition in long-term cultures. The actin cytoskeleton arranged with the fiber direction, resulting in stochastic orientation of cellular actin bundles of cells grown on random fibers (Fig. 6 A) or in a uniform linear pattern in cells on aligned fibers, coinciding with the cell polarization (Fig. 6 B). Similarly, fibronectin (FN) secreted by cells after seven days of incubation, was mainly stochastically deposited around cells grown on random PLA/FBG fibers (Fig. 6 C). In contrast, FN matrix produced by cells grown on aligned fibers clearly assembled along the main fiber direction (Fig. 6 D). No significant difference in cell numbers was found for both random and aligned samples compared to controls after seven days of culture (Table 1).

3.6 Nitric oxide secretion

To learn whether the NFs organization may affect the functional activity of HUVEC we monitored the secretion of nitric oxide (NO) at two different time points. After one day of culture, no difference in NO secretion was found between random and aligned samples (Fig. 7 A). Two days later however, the

cells cultured on random fibers secreted significantly higher amounts of NO than cells on aligned fibers (Fig. 7 B)

4. Discussion

In a previous work (Gugutkov et al 2013), we have developed pure FBG nanofibers via electrospinning, a method that has been repetitively used to create ultrathin fibers from a variety of matrix proteins (Wnek et al 2003, Perumcherry et al 2011). While pure FBG fibers were well-recognized by endothelial cells, they had poor mechanical properties which hamper their application as scaffold material in vascular tissue engineering. Therefore, we here describe a novel type of hybrid FBG/PLA nanofibers with strongly improved mechanical stability, but retaining the favorable cell recognition properties of native FBG.

Utilizing established protocols (Wenek et al 2003; He et al 2011; Perumcherry et al 2011) we obtained fibers with an average diameter of 300 nm that compared well with other FBG-based nanofibers (He et al., 2011). However, we observe that the diameter of aligned fibers is more heterogeneous than random fibers, presumably because of the turbulence forces caused from the rotating collector, resulting that the small fibers are less oriented.

Three important aspects of our composite FBG/PLA fibers need to be clarified: (i) the influence of the electrospinning process on the protein structure, (ii) the long-term stability of the electrospun fibers in physiological environment and (iii) the improved biomechanical properties of these nanofibers. In this context, one has to consider that it is still not clear how FBG becomes insoluble during electrospinning. One possibility would be that FBG is cleaved to fibrin if traces

of thrombin are present in commercially available FBG. However, in a previous work (Gugutkov et al, 2013) we excluded that possibility by showing that FBG did not convert to fibrin during electrospinning, as not displaying the typical electrophoretic band (between B′β′ and γ) present in fibrin and caused by fibrinopeptide loss from the polymer backbone (Mosesson, 2005). We thus hypothesize that electrospinning provides conditions where FBG molecules convert to an insoluble form by attractive van der Waals forces that overcome the electrostatic forces of repulsion. It should also be kept in mind that an insoluble FBG exists also in nature, as extrahepatic FBG can assemble into insoluble matrix fibrils in presence of cells, such as lung and mammary epithelial cells (Pereira et al 2002; Rybarczyk et al, 2003). In that case, cells are presumed to be involved in a process where cryptic beta residues are exposed to form FBG fibrils (Rybarczyk et al, 2003). Although the relevance of such an assembly mechanism in absence of cells is not clear, it may have consequences for the long-term stability of the nanofibers. We therefore used fluorescently labelled FBG (FITC-FBG) and traced the release of FITC from the fibers as they were exposed to physiological conditions.

Due to difficulties to measure the initial amount of protein in the fibers (tightly packed FBG molecules cannot be completely extracted) we had to measure the relative loss of FITC-FBG into the medium, comparing with pure FBG nanofibers as control. Both FITC-FBG/PLA and FITC-FBG nanofibers had similar release kinetics of FITC-FBG, indicating entrapment stability of FBG. Considering, as previously shown that approximately 5% of the protein from pure FBG fibers dissolves within 1 week (Gugutkov et al, 2013), we concluded

that the protein is stably incorporated within the polymer backbone and that the composite FBG/PLA fibers are sufficiently stable in physiological conditions.

Regarding the biomechanical properties, composite FBG/PLA nanofibers were significantly stiffer than pure FBG nanofibers but much softer than pure PLA fibers when measured in dry state. It should be emphasized however that pure FBG nanofibers possessed extremely poor mechanical properties when immersed in wet conditions. Their elastic modulus decreases more than 1000 times (detailed by Baker et al. 2012), which makes their applicability in tissue engineering really questionable. For example, in our previous studies we could not introduce pure FBG fibers to the dorsal cell surface of HUVECs as fibers broke immediately upon contact with water surface. However, the elastic modulus of the new FBG/PLA fibers increased more than 100 times (Fig. 2B), which in fact, made possible the artificial wound settings described in this study (where we apply fibers over the cells layer through the medium). To our view, it is the main advantage of the FBG/PLA nanofibers: they combine the very good mechanical properties of PLA with the excellent biological properties of native FBG. In this context, though the technological aspects of producing artificial vessels are out of the scope of this paper, we would like to emphasize that now we succeed in producing tubular structures using randomly deposited electrospun FBG/PLA nanofibers (over the rotating 2 mm metal drum stick), which was not possible with pure FBG ones (see supplementary Figure 1). Moreover the surface of this scaffold is less thrombogenic by means of a lowered platelet aggregation at the surface of composite FBG/PLA nanofibers (whole blood test) in comparison to the pure FBG ones, thus acquiring surface

properties similar to the relatively inert pure PLA fibers (see supplementary Figure 2).

However, despite the promise of the composite fibrous scaffold, there is still a need to understand how cells respond to the spatial orientation of NFs providing obviously “readable” biological cues. Therefore, another issue we want to stress on here is the morphological response of adhering endothelial cells to the nanofibers. We found clear differences in the overall cell morphology depending on the spatial organization of fibers. On aligned fibers, cells presented an extended morphology that strongly followed the fiber orientation, while on random ones they spread in multiple directions. It is well documented that despite belonging to a common type, the cells display a variety of shapes depending on the geometry of adhesive environment on which they adapt their cytoskeleton (Théry et al, 2006). Indeed, the presence of highly extended actin stress fibers inserting into focal adhesions suggests that endothelial cells exert significant traction over the FBG-PLA fibers. Interestingly, the overall shape of HUVECs on random fibers resembles to some extent the stellate-like morphology characteristic for cells residing in three dimensional environments (Grinnell, 2003). This leads to the conviction that endothelial cells can “read” the geometry of the underlining nanofibers, and because they cannot enter between fibers they perceive them rather as topography (i.e. 2.5D). It should be emphasized however that the appearance of well-established matrix contacts suggests that FBG/PLA nanofibers provide enough ligand density for clustering of integrins, i.e. spaced in a less than 60-70 nm distance, required for the assembly of focal complexes (Geiger et al. 2009). Collectively, this study

provides morphological evidence that endothelial cells interact very well with the composite FBG/PLA fibers which set them among the prospective biomimetic scaffolds for vascular tissue engineering.

Beyond the events of initial morphological response, the time-lapse studies revealed that cell migration patterns also depended on the spatial orientation of nanofibers. Understanding the factors that control cell migration is, in general, a key issue when designing implants for optimal integration with native tissue. In accordance with other studies (Sundararaghavan et al, 2013) here we show that HUVECs not only oriented themselves to aligned nanofibers, but also migrated along them. The difference in cell migration on aligned fibers compared to randomly oriented fibers was particularly dramatic in the artificial wounds experiments, where aligned fibers were dorsally applied over the cells. In that case HUVECs migrated towards the empty regions of the wound, resulting in fast wound coverage. Conversely, when adhering to randomly deposited fibers, or when overlaid with them in the wound experiments, the cells were locally immobilized, most probably because of their anchorage with multiple projections. Nevertheless, while guided directional cell movement might be important for recruitment of endothelial cells on scaffolds promoting angiogenesis, local immobilization of cells on randomly organized fibers could also be of interest, e.g. for endothelization of blood contacting devices where the up-regulation of the adhesive machinery is very important (de Mel et al 2008). While tissue neovascularization and integration of many implants with the host circulation still remains a major barrier for transplantation of engineered tissues - a field that has not yet identified an effective strategy (Lovett et al,

2009) - nanofibers that efficiently guide cell migration could be an important tool. Indeed, recent progress in this field suggests that allowing vascular cells to form oriented rudimentary vascular networks either *in vitro* (prevascularization) or *in vivo* might results in enhanced integration of grafted endothelial cells with host vasculature (Kang and Bischoff 2011; Baranski et al, 2013). Our studies contribute to the field showing that an oriented nanofibrous scaffold can be used as a tool for guided vascularization of implant. In addition we show that the balance of adhesive and motile phenotypes influences endothelial cells functionality. In particular, we found that the orientations of the underlying nanofibers clearly reflected in the organization of the confluent cell layers. Not only was the cellular actin cytoskeleton well-aligned with the fiber direction, but the newly generated fibronectin matrix fibrils also followed it organization along the nanofiber direction. Those observations suggest that nanofibers orientation might be a key to regulated fibronectin matrix assembly, which may serve as a template for tailored ECM deposition. Interestingly, although cells grew equally well on both type of nanofibers (Table 1), randomly oriented nanofibers provoked endothelial cells to produce significantly more NO, allowing cells to better influence local vessel contractility and platelet activation (Förstermann and Münzel, 2006).

Conclusion

We report on successful electrospinning of novel composite FBG/PLA nanofibers that combine good biomechanical properties of PLA with excellent cell recognition properties of native FBG. Random nanofibers provoked a stellate-like morphology of endothelial cells with multiple cytoplasmic projections, which made them relatively immobile. Conversely, an elongated cell shape combined with a significantly increased cell mobility and faster wound coverage were observed on aligned NFs. However, NO release assay showed that HUVECs possessed lower functionality on aligned NFs compared to the randomly deposited ones. Collectively, our studies show that randomly organized NFs may support the endothelization of blood contacting devices while aligned ones could provide a tool for guided neovascularization of implants.

Acknowledgements

This work was supported by CIBER-BBN (Spain) and the European Commission through the FP7 Industry-Academia Partnerships and Pathways (IAPP) project FIBROGELNET and the EuroNanoMed project STRUCTGEL. The valuable support of the project MAT2012-38359-C03-03 HEALINSYNERGY, funded by Spanish Ministry of Science and Innovation is also acknowledged.

References

1. Arnold M, Cavalcanti-Adam A, Glass R, Blmmel J, Eck W, Kessler H and Spatz J. 2004, Activation of integrin function by nanopaterned adhesive interfaces, *Chem. Phys. Chem*, **3**: 383-388

2. Baji A, Mai YM, Wong SC, Abtahi M, Chen P. 2010, Electrospinning polymer nanofibers: Effects on oriented morphology, structures and tensile properties, *Compos. Sci. Technol.*, **70(5)**: 703-718

3. Baker S, Sigley J, Carlisle CR, Stitzel J, Berry J, Bonin K, Guthold, 2012. The Mechanical Properties of Dry, Electrospun Fibrinogen Fibers, *Mater Sci Eng C Mater Biol Appl*,**1;32(2)**: 215-221

4. Baranski JD, Chaturvedi RR, Stevens KR, Eyckmans J, Carvalho B, Solorzano RD, Yang MT, Miller JS, Bhatia SN, Chen CS. 2013, Geometric control of vascular networks to enhance engineered tissue integration and function, *Proc Natl Acad Sci U S A*, **110(19)**:7586-7591

5. Chiu JB, Luu YK, Fang D, Hasiao B, Chu B, Hadjiargyurou. 2005, Electrospun nanofibrous scaffold for Biomedical Applications, *J Biomed Nanotechgnol*. **1**: 115-123

6. Cleary MA, Geiger E, Grady C, Best C, Naito Y, Breuer C. 2012, Vascular tissue engineering: the next generation, *Trend Mol Med*,**18 (7)**: 394-404

7. De Mel A, Jell G, Stevens MM, Seifalian AM. 2008, Biofunctionalization of biomaterials for accelerated in situ endothelialization: a review,

Biomacromolecules, **9(11)**: 2969-2979

8. Dvir T, Timko BP, Kohane S, R. Langer. 2010, Naniotechnological strategies for engineering complex tissues, *Nature Nanotech*, **6**: 13-22

9. Edelman RE. 1999, Vascular tissue engineering: designer arteries, *Circ Res*. **85**: 1115-1117

10. Fang J, Wang X, Lin T, 2011. 'Functional Applications of Electrospun Nanofibers' in *Nanofibers - Production, Properties and Functional Applications*, eds. Dr. Tong Lin, InTech, 285-326

11. Forner L, Salmerón-Sánchez M, Palomares M, Llena C, Amengual J. 2009, The use of atomic force microscopy in determining the stiffness and adhesion force of human dentin after exposure to bleaching agents, J Endod, **35(10)**: 1384-1386

12. Förstermann U, Münzel T. 2006, Endothelial nitric oxide synthase in vascular disease: from marvel to menace, *Circulation*, **113(13)**: 1708-1714

13. Fu X, Wang H. 2012, Spatial arrangement of polycaprolactone/collagen nanofiber scaffolds regulates the wound healing related behaviors of human adipose stromal cells, *Tissue Eng, Part A*, **18**: 631-642

14. Geiger B, Spatz JP, Bershadsky AD. 2009, Environmental sensing through focal adhesions, *Nat Rev Mol Cell Biol*, **10(1)**: 21-33

15. Grinnell F. 2003, Fibroblast biology in three-dimensional collagen

matrices. *Trends Cell Biol*, **13(5)**: 264-269

16. Guelcher SA, Goldstein AS. 2009, Effect of fiber diameter and alignment of electrospun polyurethane meshes on meshenchimal progenitor cells, *Tissue Eng Partr A*, **15**: 2435-2445

17. Gugutkov D, Gustavsson J, Ginebra MP, Altankov G. 2013, Fibrinogen nanofibers for guiding endothelial cells behavior, *Biomater Sci*, **1**: 1065-1073

18. He Ch, Xi X, Zhang F, Cao L, Feng W, Wang H, Mo X. 2011, Fabrication of fi brinogen/P(LLA-CL) hybrid nanofibrous scaffold for potential soft engineering application, *J Biomed Mater. Res A*, **97A(3)**: 339-347

19. Kang K-T, Bischoff J. 2011, Bioengineered human vascular networks transplanted into secondary mice reconnect with the host vasculature and re-establish perfusion, *Blood*, **118(25)**: 6718-6721

20. Kumar TRS, Krishnan LK. 2001, ECGF enmeshed with fibrin matrix enhances proliferation of EC in vitro, *Biomaterials*, **22**: 2769-2776

21. Liu H, Ding X, Zhou G, Li P, Wei X, Fan Y. 2013, Electrospinning of Nanofibers for Tissue Engineering Applications, *Journal of Nanomaterials*, **10.1155/2013/495708**

22. Liu Y, Ji Y, Chosh K, Clark AF, Huang L, Rafailovitch MH. 2009, Effects of fiber orientation and diameter on the behavior of human dermal fibroblasts on electrospun PMMA scaffolds, *J Biomed Mater Res, Part A*,

90: 1092-2009

23. Lovett M, Lee K, Edwards A, Kaplan DL. 2009, Vascularization strategies for tissue engineering, *Tissue Eng part B Rev*, **15(3)**: 353-370

24. Lutolf MP, Hubbell JA. 2005, Synthetic biomaterials as instructive extracellular microenvironments for morphogenesis in tissue engineering, *Nature Biotech*., **23 (1)**: 47-55

25. Ma, Z, Kotaki M, Yong T, He W, Ramakrishna S. 2005, Surface Engineering of electrospun Polyethylene Tetraphthalate nanofibers towards development of a new material for blood vessels engineering, *Biomaterials*, **26**: 2527-2536

26. Mosesson MW. 2005, Fibrinogen and fibrin structure and functions, *J. Thromb. Haemostasis*, **3**: 1894-1904

27. Nisbet DR, Pattanawong S, Ritchie NE, Shen W, Funkelstein DI, Horne MK, Forsythe JS. 2007, Interaction of embryonic cortical neurons on nanofibrous scaffolds for neuronal tissue engineering, *J Neuronal Engin*, **4**: 35-41

28. Pereira M, Rybarczyk BJ, Odrljin TM, Hocking DC, Sottile J, Simpson-Haidaris PJ. 2002, The incorporation of fibrinogen into extracellular matrix is dependent on active assembly of a fibronectin matrix. *J Cell Sci*; **115(Pt 3)**: 609-617

29. Perumcherry SR, Chennazahi KP, Nair SV, Menon D, Tech AB. 2011, A

novel method for fabrication of fibrin-based electrospun nanofibrous scaffold for tissue-engineering application, *Tissue Eng. Part C*, **17(11)**: 1-10

30. Rybarczyk BJ, Lawrence SO, Simpson-Haidaris P J. 2003, Matrix-fibrinogen enhances wound closure by increasing both cell proliferation and migration, *Blood*, **102**: 4035

31. Stevens MM, George JH. 2005, Exploring and engineering the Cell Surface Interface, *Science*, **310**: 1135-1138

32. Sundararaghavan HG, Saunders RL, Hammer DA, Burdick JA. 2013, Fiber alignment directs cell motility over chemotactic gradients. *Biotechnol Bioeng*, **110(4)**:1249-54

33. Swartz DD, Russell JA, Andreadis ST. 2005, Engineering of fibrin-based functional and implantable small-diameter blood vessels, *Am J Physiol Heart Circ Physiol*, **288(3)**:1451-1460

34. Théry M, Pépin A, Dressaire E, Chen Y, Bornens M. 2006, Cell distribution of stress fibres in response to the geometry of the adhesive environment. *Cell Motil Cytoskeleton*, **63(6)**: 341-55

35. Wade RJ, Burdick IA. 2012, Engineering ECM signals into biomaterials. *Mater Today*, **15**: 454-459

36. Wnek GE, Carr ME, Simpson DG, GL Bowlin (2003) Electrospinning of nanofiber fibrinogen structure, *Nano Lett*, **3**: 213-216.

	FBG coated glass	FBG/PLA nanofibers	
		random	aligned
Average number of cells per square	100.25	88.5	89.25
Standard deviation	14.00	7.33	6.29

Table 1. Cell density at seventh day of culture on random and aligned nanofibers compared to control values (FBG-coated glass). Data represent number of nuclei per microscopic field (magnification 20x, n=4)

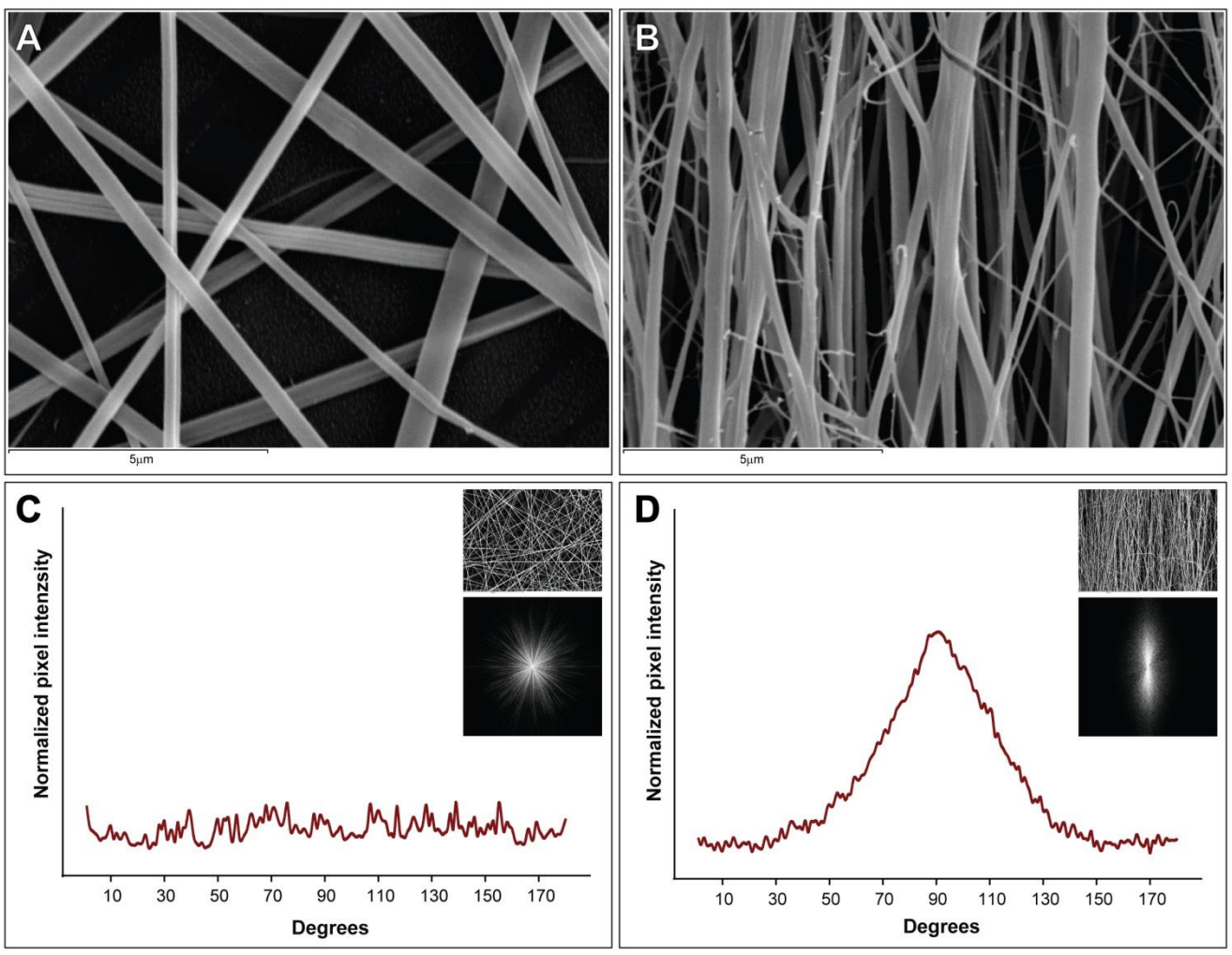

Figure 1. SEM images representing the spatial organization of electrospun FBG/PLA nanofibers in random (A) and aligned (B) configuration.The spatial organization of fibers was characterized by FFT analysis and plotted as pixel intensity against the angle of acquisition (C and D).The pick of intensity around 90^0 indicates the fibers alignment (D), which is not presented in random samples (C).

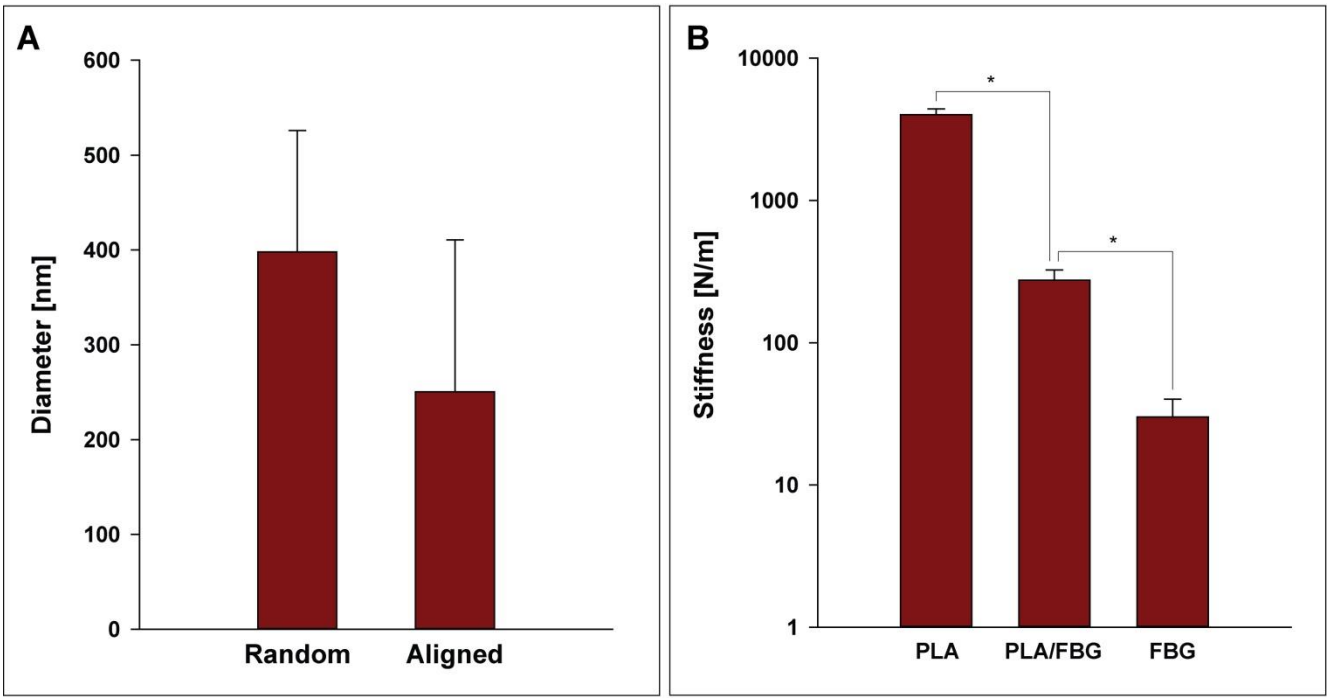

Figure 2. Average fibers diameter (A) and stiffness (B) of composite FBG/PLA nanofibers compared with plane FBG and PLA fibers.

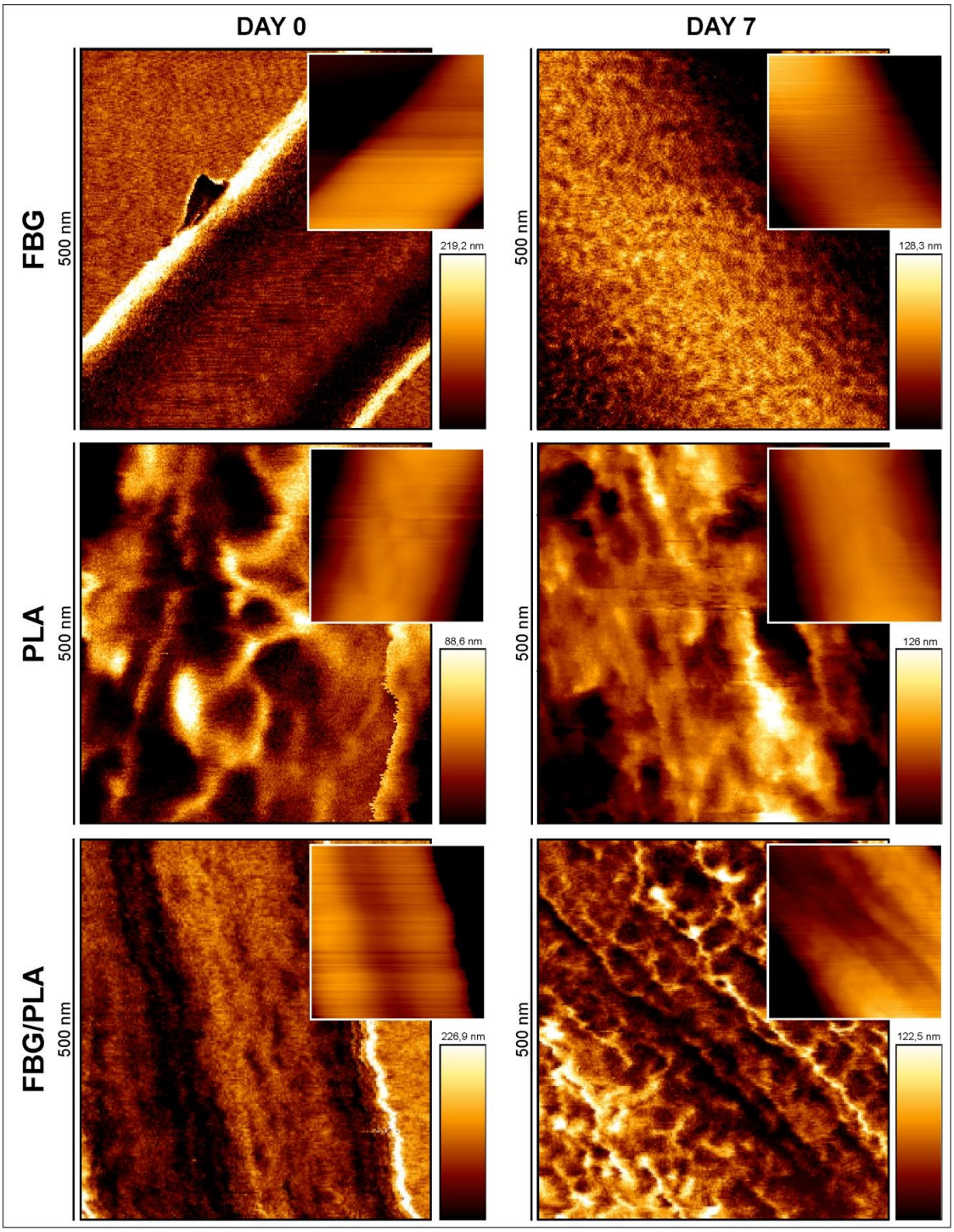

Figure 3. AFM adhesion images of pure FBG (upper row), pure PLA (second row) and composite FBG/PLA nanofibers (bottom row) at DAY 1 (left column) and at DAY 7 (right column), i.e. after incubation of samples for 1 week in PBS. No signs of degradation were observed for the pure PLA samples, but slightly rougher surfaces can be obtained on pure FBG and composite FBG/PLA fibers after 1 week of incubation. However, from the inserts, showing AFM height images of the same samples, a rather disparaging morphology was observed, implying on a very little degradation.

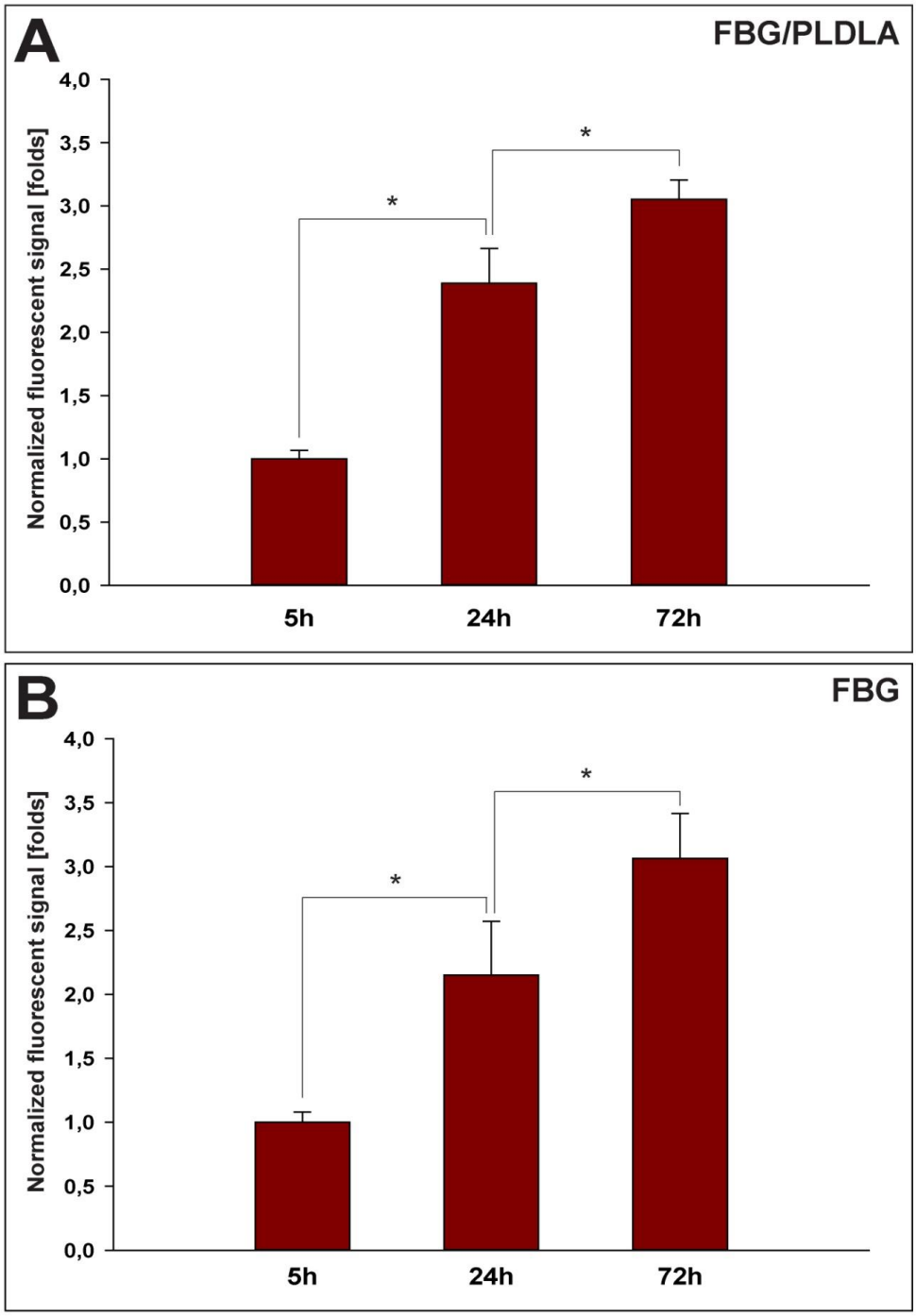

Figure 4. Characterization of the stability of electrospun FBG fibers. Kinetics of FITC- FBG release from composite FBG/PLA (A) and pure FBG (B) samples. Fibers containing 1% FITC-labeled FBG were incubated for 5, 24 and 72 hours in PBS and fluorescent intensity [CPS] of supernatants was measured. The values for 24 and 72 hours were normalized to the signal of 5 h accepted as reference.

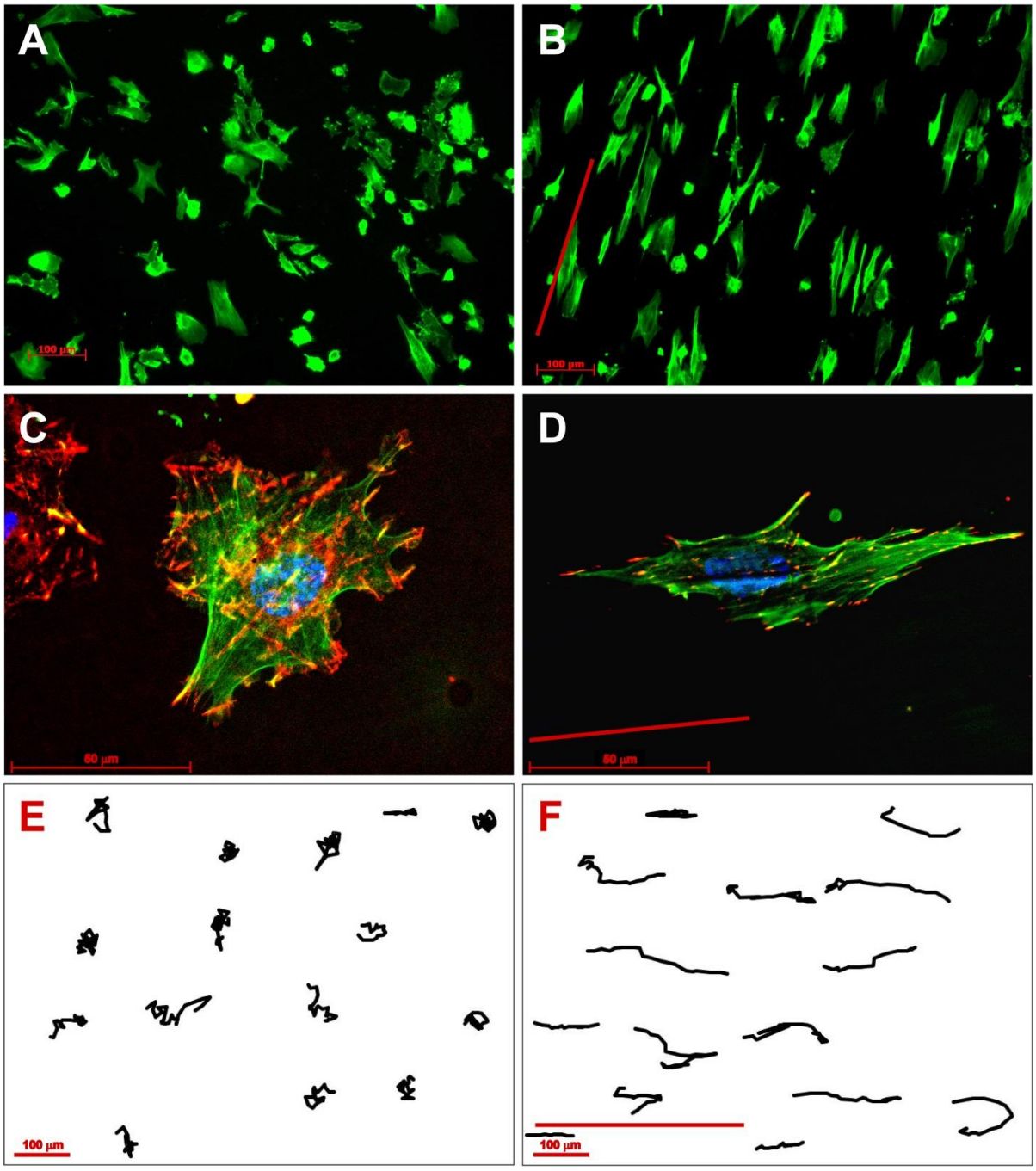

Figure 5. Cellular interactions with FBG/PLDLA nanofibers.
A, B: Overall morphology of HUVECs after 2 hours of incubation on random (A) or aligned (B) nanofibers.
C, D: Visualization of focal adhesion complexes by vinculin (red) and actin cytoskeleton (green) on random (C), and aligned nanofibers (D). Nuclei are stained by Hoechst (blue).
E, F: Visualization of cell tracks on random (E) and aligned nanofibers (F). Time laps were recorded at phase contrast(magnification 10x); the direction of fibers alignment (if any) is indicated with red line.

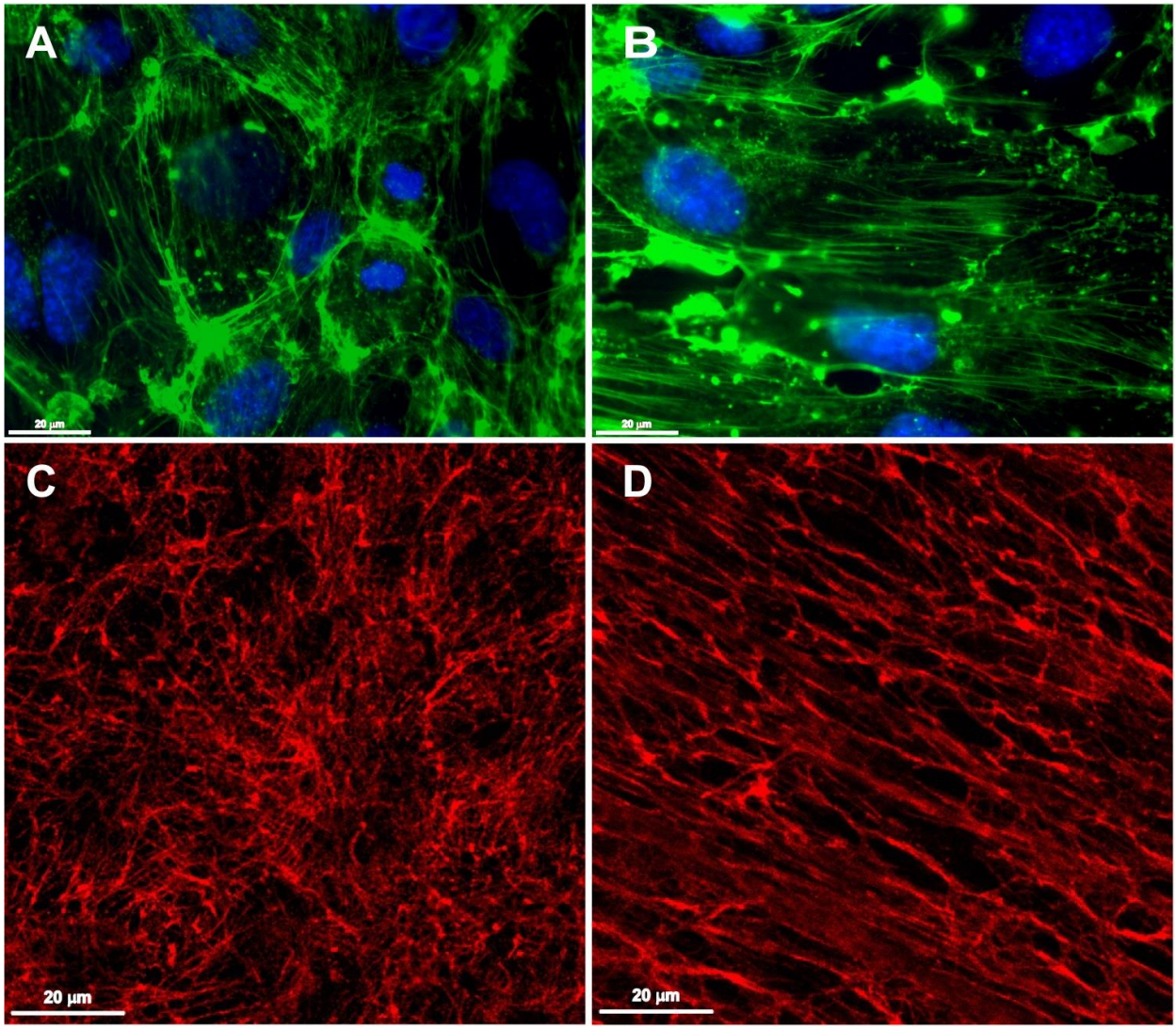

Figure 6. Indirect imunofluorescent staining HUVEC cultured for 7 days on random (A) and aligned FBG nanofibers (B) by phalloidin (green actin) and Hoescht (blue nuclei). Deposition of fibronectin secreted by HUVECs cultured for 7 days on random (C) and aligned FBG/PLDLA nanofibers (D).

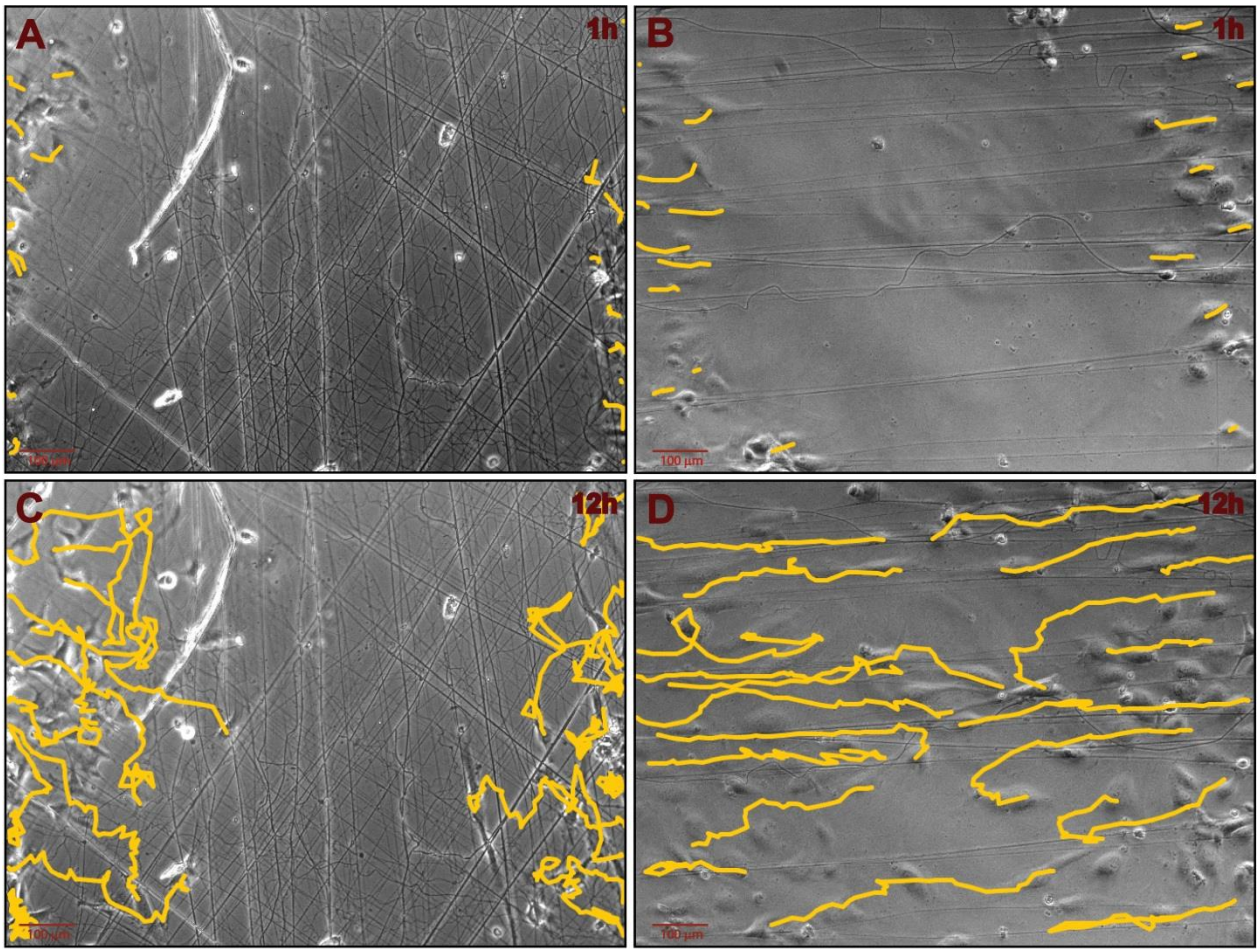

Figure 7. Cell-tracks analysis during wound healing experiment Random (A, C) and aligned (B,D) FBG/PLA nanofibers were applied onto the dorsal cell surface of confluent HUVECs layer where previously artificial wounds were created (see Methods section). Cell tracks (in yellow) were obtained by analysis of the time-laps movies (MTrack, ImageJ) during the 1st hour (A, C) and 12 hours (C,D) of incubation.

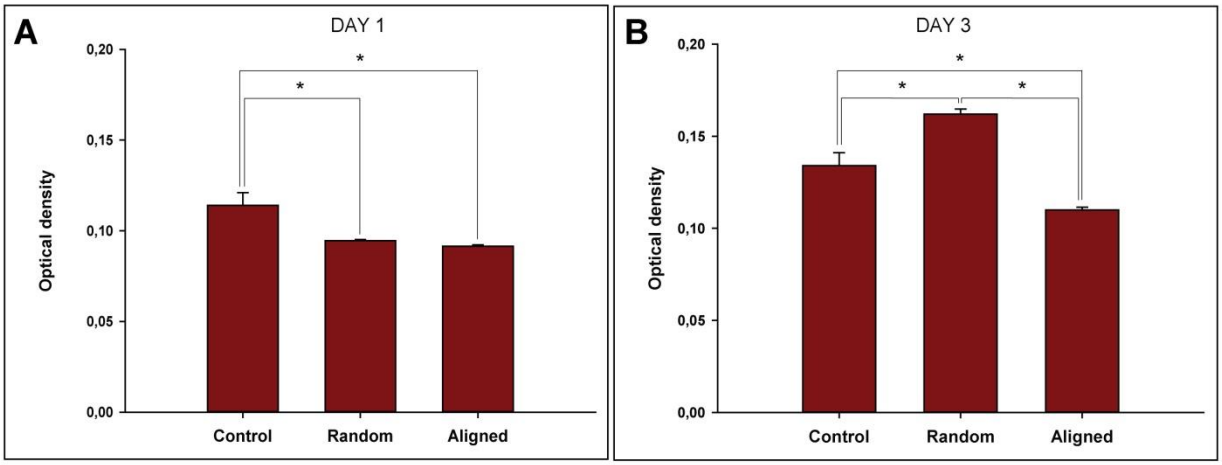

Figure 8. Nitric oxide production of HUVECS cultured onto FBG/PLA nanofibers at DAY 1 (A) and DAY 3 (B) of incubation. The photometric signals were normalized to the main number of cells (nuclei density counted in 4 randomly chosen microscopic fields).

	FBG coated glass	FBG/PLA nanofibers random	FBG/PLA nanofibers aligned
Average number of cells per	100,25	88,5	89,25
Standard deviation	14,00	7,33	6,29
Total number of cells	401	354	357

Table1. Cell density after 7 days of culture.